Pervasive generation of non-canonical subgenomic RNAs by SARS-CoV-2

Jason Nomburg[1,2,3], Matthew Meyerson[1,2,4,5*], James A. DeCaprio[1,3,5*]

[1]Department of Medical Oncology, Dana-Farber Cancer Institute, Boston MA

[2]Broad Institute of MIT and Harvard, Cambridge, MA

[3]Harvard Program in Virology, Harvard University Graduate School of Arts and Sciences, Boston, MA

[4]Department of Genetics, Harvard Medical School, Boston, MA

[5]Department of Medicine, Brigham and Women's Hospital, Harvard Medical School, Boston, MA

*Correspondence to:

James A. DeCaprio

james_decaprio@dfci.harvard.edu

Matthew Meyerson

matthew_meyerson@dfci.harvard.edu

Abstract

Background: SARS-CoV-2, a positive-sense RNA virus in the family *Coronaviridae*, has caused a worldwide pandemic of coronavirus disease 2019 or COVID-19 Coronaviruses generate a tiered series of subgenomic RNAs (sgRNAs) through a process involving homology between transcriptional regulatory sequences (TRS) located after the leader sequence in the 5' UTR (the TRS-L) and TRS' located near the start of structural and accessory proteins (TRS-B) near the 3' end of the genome. In addition to the canonical sgRNAs generated by SARS-CoV-2, non-canonical sgRNAs (nc-sgRNAs) have been reported. However, the consistency of these nc-sgRNAs across viral isolates and infection conditions is unknown. The comprehensive definition of SARS-CoV-2 RNA products is a key step in understanding SARS-CoV-2 pathogenesis.

Methods: Here, we report an integrative analysis of eight independent SARS-CoV-2 transcriptomes generated using three sequencing strategies, five host systems, and seven viral isolates. Read-mapping to the SARS-CoV-2 genome was used to determine the 5' and 3' coordinates of all identified junctions in viral RNAs identified in these samples.

Results: Using junctional abundances, we show nc-sgRNAs make up as much as 33% of total sgRNAs *in vitro*, are largely consistent in abundance across independent transcriptomes, and increase in abundance over time during *in vitro* infection. By

assessing the homology between sequences flanking the 5' and 3' junction points, we show that nc-sgRNAs are not associated with TRS-like homology. By incorporating read coverage information, we find strong evidence for subgenomic RNAs that contain only 5' regions of ORF1a. Finally, we show that non-canonical junctions change the landscape of viral open reading frames.

Conclusions: We identify canonical and non-canonical junctions in SARS-CoV-2 sgRNAs and show that these RNA products are consistently generated across many independent viral isolates and sequencing approaches. These analyses highlight the diverse transcriptional activity of SARS-CoV-2 and offer important insights into SARS-CoV-2 biology.

Key Words

SARS-CoV-2, COVID-19, direct RNA sequencing, transcription

Background

Severe acute respiratory syndrome coronavirus 2 (SARS-CoV-2) emerged from Wuhan, China in December 2019 and rapidly led to a world-wide pandemic, known as COVID-19 (1). The initial sequencing report found that this virus maintains 89.1% nucleotide identity to SARS-like coronaviruses found in bats in China (1).

Coronaviruses (CoV) including SARS-CoV-2 contain large, ~ 30kb, positive-sense, single-stranded RNA genomes with a unique genome organization structure. The 5' end of the genome contains two large open reading frames (ORFs), ORF1a and ORF1b. ORF1a produces a large polyprotein, while ribosomal slippage at an RNA pseudoknot structure and slippery sequence at the end of ORF1a occasionally leads to a frameshift and subsequent translation of a joint ORF1a and ORF1b polyprotein (2). ORF1a and ORF1ab polyproteins contain protease activity that can cleave the polyproteins into a variety of nonstructural proteins (Nsp) capable of facilitating viral transcription and replication and modulating host transcription and translation. Following ORF1b, there is an arrangement of ORFs encoding structural and accessory proteins that tend to vary in content and order across the CoV family. While structural proteins are incorporated into emergent virions, accessory proteins are thought to be dispensable for replication *in vitro* but to increase fitness *in vivo* (3-5).

Initial translation of ORF1ab can occur directly from incoming viral genomic RNA, generating the ORF1a and ORF1ab polyproteins and initiating infection. However, because the viral genome is so large, and because downstream ORFs are far from the

82 5’ end of the genome, effective translation of these ORFs requires the generation of
83 subgenomic RNAs (sgRNAs) (6). To generate these sgRNAs, it is thought that CoV
84 undergoes a process of discontinuous extension during synthesis of negative-stranded
85 RNA templates. As the virus-encoded RNA-dependent RNA polymerase progresses
86 from the 3’ end towards the 5’ end of the viral genome, it encounters transcriptional
87 regulatory sequences (TRS) upstream of each major ORF (TRS-B). Here, the
88 polymerase can skip to a similar TRS that is 3’ of a shared leader sequence within the
89 5’ UTR of the CoV genome (TRS-L). These antisense sgRNAs are then transcribed,
90 resulting in a series of tiered sgRNAs containing the same 5’ leader sequence (6).
91
92 Several studies have characterized SARS-CoV-2 sgRNAs using Nanopore direct RNA
93 sequencing (dRNAseq). In contrast to short-read sequencing, which can produce read
94 pairs of 150bp each, dRNAseq is capable of directly sequencing entire transcripts
95 including the full length of the viral genome (29903 bases). This allows dRNAseq to
96 identify RNA isoforms and variants that may be challenging to deconvolute using short-
97 read sequencing. Using nanopore sequencing, Taiaroa et al. identified eight major
98 sgRNAs, as well as a small number of non-canonical junctions between the 5’ leader
99 sequence and downstream regions of the SARS-CoV-2 genome (7). Kim et al. identified
100 a total of 9 distinct subgenomic RNAs, as well as a series of non-canonical subgenomic
101 RNAs (nc-sgRNAs) that contain unexpected junctions between 5’ and 3’ sequences (8).
102 Using short-read DNA nanoball sequencing data, they confirmed the existence of
103 noncanonical junctions at various sites across the genome (8). Davidson et al. identified

104 a series of transcripts encoding the nucleocapsid (N) protein, but with distinct small
105 internal deletions, and validated this finding with proteomic evidence (9).
106
107 While these previous studies identified non-canonical RNA junctions and unexpected
108 RNA species in isolation, there were no integrative analyses of the SARS-CoV-2
109 junctions. It is unclear if identified non-canonical junctions are broadly representative of
110 SARS-CoV-2 biology or if they are a result of dataset- or isolate-specific artifacts. Here,
111 we report an integrative analysis of eight independent SARS-CoV-2 transcriptomes
112 generated using three sequencing strategies, five host systems, and seven viral isolates
113 to comprehensively characterize the landscape of canonical and non-canonical sgRNAs
114 generated by SARS-CoV-2.
115

116 Results

117 **Analysis of three independent dRNAseq datasets reveals canonical and**
118 **noncanonical junctions.**
119 To determine the major RNA species present in SARS-CoV-2-infected cells, we applied
120 a uniform computational approach to three independent dRNAseq datasets from
121 Taiaroa et al., Kim et al., and Davidson et al. (7, 10, 11). To assess sgRNA presence,
122 we identified junction-spanning reads following read-mapping against the SARS-CoV-2
123 reference genome.
124
125 Analysis of the 5' and 3' locations of junctions separated by at least 1000 bases
126 revealed that the majority of junctions consist of a 5' end originating in the 5' UTR and a

127 3’ end at distinct sites in the 3’ region of the genome (**Figure 1A-C**). These represent
128 the canonical junctions between the leader sequence and 3’ sequences that generate
129 the major sgRNAs (6)**.** Plotting the counts of 3’ junctions that contain a 5’ end within the
130 first 100 bases revealed eight prevalent junction points along the 3’ end of the genome
131 (**Figure 1D-F**), all of which are proximal to the TRS core sequence ACGAAC.
132 Interestingly, we observed that the 3’ junction peak and TRS-B closest to ORF6 lands
133 151 bases within the M ORF. Based on these junction analyses and the locations of
134 identified TRS body sites, predicted sgRNAs and their most 5’ gene or genes are shown
135 in **Figure 1G**. We predict 8 major sgRNAs based both on identification of the TRS core
136 sequence and presence of a dominant junction peak. In contrast to Kim et al. (8) but in
137 concordance with Taiaroa et al. (7) and Davidson et al. (9), we do not find evidence of a
138 prominent 3’ junction point near ORF7B (**Figure 1D-F**).
139
140 **Many SARS-CoV-2 junctions are non-canonical.**
141 Similar to observations by Kim et al. (8), we identified an unexpectedly diffuse pattern of
142 noncanonical junctions across the genome (**Figure 1A-C**, black arcs), suggesting that
143 there are many unexpected RNA species. Had there been only canonical junctions, the
144 arcs on this plot would be exclusively between the first 100 bases and defined points on
145 the x-axis (**Figure 1A-F**).
146
147 Because the transcriptomes in these long-read sequencing studies (7, 8, 11) all consist
148 of dRNAseq from infected Vero cells, we sought to confirm this observation in
149 independent transcriptomes from other SARS-CoV-2 isolates, in other host systems,

150 and using other sequencing technologies. To this end, we assessed five additional
151 transcriptomes generated from Vero cells (12), A549 cells (13), Calu3 cells (14),
152 bronchial organoids (15), and ferret nasal washings (13) using Illumina PolyA or total
153 RNA sequencing. Detailed information regarding each sample is detailed in the
154 methods. Junction analysis in these transcriptomes likewise revealed pervasive non-
155 canonical junctions (**Supplementary Figure 1A-E**). Quantification of the relative
156 abundance of canonical and non-canonical junctions in these transcriptomes revealed
157 that up to 33% of junctions are non-canonical *in vitro* (**Figure 2A, Supplementary**
158 **Figure 1F**). The transcriptome from a ferret's nasal washing contained 51% non-
159 canonical junctions, indicating that non-canonical junctions are also produced *in vivo*.
160
161 We sought to assess if non-canonical junctions are driven by dataset-specific artifacts.
162 For example, it is possible that defective particles containing defective viral genomes
163 (DVGs), often with large internal deletions that increase their replicative fitness, could
164 accumulate during preparation of virion stocks (16) and generate the observed non-
165 canonical junctions during subsequent infections. If this was true, we would expect to
166 observe non-canonical junctions specific to a single virion preparation and accumulation
167 of these specific non-canonical junctions over the course of infection. To address this
168 possibility, we identified dataset-specific junctions by identifying junctions that are
169 differentially abundant across datasets (**Figure 2B)**. This analysis revealed that the vast
170 majority of 5' and 3' non-canonical junctions are low abundance and are similarly
171 abundant across five independent SARS-CoV-2 sequencing studies (7-9, 12, 13)

172 (**Figure 2C, D**). This suggests that most non-canonical junctions are not driven by
173 dataset-specific artifacts.
174
175 However, we found that three 5' junction sites in the Finkel et al. transcriptome and
176 three 3' junctions in the Davidson et al. transcriptome were overrepresented (**Figure**
177 **2C, D**). Incorporating additional replicates of these transcriptomes and assessing the
178 percentage of non-canonical junctions at each site revealed that the Finkel et al.-
179 specific 5' junctions are highly elevated in both Finkel et al. replicates relative to other
180 transcriptomes (**Supplementary Figure 3A-C**). In contrast, the three Davidson et al.-
181 specific 3' junctions are present in other datasets but at slightly lower frequency
182 (**Supplementary Figure 3D, E**). The consistency of the Finkel et al.-specific junctions
183 across replicates and exclusion from other samples raises the possibility that these
184 junctions were generated from defective particles in the Finkel et al. virion preparation.
185
186 **The proportion of non-canonical junctions increases over time *in vitro*.**
187 Next, we assessed changes in junctions over time using the approach detailed in
188 **Figure 3A** using transcriptomes from early (4 or 5 hours post infection) and late (24
189 hours post infection) timepoints from Finkel et al. (12) and Emanual et al. (14). This
190 analysis revealed that there are large decreases in 5' junctions originating at position
191 64, and in 3' junctions ending in 28254 (proximal to the N TRS-B), with a smaller
192 decrease in 3' junctions ending at 26467 (proximal to the M TRS-B) (**Figure 3B,C**).
193 Notably, the Finkel et al.-specific 5' junction at 16971 increased in abundance over time.
194 In contrast, there were no specific large increases in percentage of junctions at other

195 positions (**Figure 3B,C**). Instead, there are small but widespread increases in non-
196 canonical junction sites throughout the SARS-CoV-2 genome (**Figure 3D, E**).
197 Quantification of the total percent changes of canonical and non-canonical junctions
198 revealed a large decrease in canonical N junctions and increase in non-canonical
199 junctions (**Figure 3F, G**). These results indicate that the abundance of non-canonical
200 junctions increases over time *in vitro*. It is unclear if a similar pattern occurs during
201 infection *in vivo*.
202
203 **Non-canonical junctions are not associated with TRS-like homology.**
204 While homology between the TRS-L and TRS-B is thought to be critical for generation
205 of canonical sgRNAs, the role of TRS-like homology in the generation of nc-sgRNAs is
206 unclear. To address this question, we determined the 30 bases surrounding the 5' and
207 3' sites of each junction and identified the longest continuous subsequence in common
208 between these sequence (**Figure 4A**). We found that junctions with a 3' end landing
209 within 15 nucleotides of a TRS-B overwhelmingly have junction homology associated
210 with variants of the TRS core sequence (**Figure 4B-D, blue**). In contrast, junctions
211 landing within ORFs and not proximal to a TRS-B do not have a prevalent homologous
212 sequence (**Figure 4B-D, red**). The exception are intra-M junctions, whose homology is
213 a consequence of the location of the ORF6 TRS within the M ORF.
214
215 While there is not a single strong motif driving non-canonical, intra-ORF junctions, it is
216 still possible that non-canonical junctions are associated with junction-specific homology
217 between the 5' and 3' junction sites. To address this possibility, we tallied the length of

218 homology between the 5’ and 3’ sites of canonical and non-canonical junctions. This
219 analysis revealed that canonical junctions have markedly longer homology lengths
220 (mean >10 bases) than non-canonical junctions (mean < 5 bases) (**Figure 4E-G**).
221 Indeed, the homology lengths of non-canonical junctions are only slightly longer than
222 homology lengths between 100,000 random pairs of SARS-CoV-2-derived 30 base
223 sequences (**Figure 4E-G**). These data indicate that non-canonical junctions are not
224 associated with TRS-like homology.
225
226 **sgRNAs containing only a 5’ region of ORF1a are produced in all studied *in vitro***
227 **and *in vivo* infection systems.**
228 Assessment of the three dRNAseq transcriptomes revealed evidence of sgRNAs that
229 contain only the 5’ region of ORF1a (**Supplementary Figure 3A**). This is similar to an
230 observation previously reported by Kim et al. (8). Inspection of read coverage of ORF1a
231 in these transcriptomes confirmed that there is elevated 5’ ORF1a coverage with
232 specific decreases in coverage concomitantly with sharp increases in junctions near
233 genome positions 1600 and 6000 (**Figure 5A-C**).
234
235 While there is clearly higher coverage of the 5’ region of ORF1a in the three dRNAseq
236 transcriptomes, it remained unclear if these 5’ ORF1a sgRNAs are a major percentage
237 of total ORF1a in the cell, or if this finding was due to a systematic bias favoring shorter
238 reads in nanopore sequencing. To address this question, we assessed ORF1a
239 coverage in four independent Illumina polyA-enriched RNAseq transcriptomes. Analysis
240 of these transcriptomes revealed a similar elevated 5’ ORF1a coverage and consistent

241 drops in coverage around genome positions 1600 and 6000 (**Figure 5D-G**). Importantly,
242 one of these transcriptomes is from bronchial organoids (**Figure 5G**) and one
243 transcriptome is from the nasal washings of an infected ferret (**Figure 5F**), suggesting
244 that 5' ORF1a subgenomic RNAs can be produced *in vivo* and were not only due to
245 artifacts of highly replicative conditions *in vitro*. Furthermore, analysis of a transcriptome
246 generated from RNA that was not polyA-enriched revealed a consistent elevation in 5'
247 ORF1a coverage (**Figure 5H**), ruling out a systematic bias from polyA isolation. We
248 found that there is similar elevated 5' ORF1a coverage in the circulating human
249 coronavirus CoV 229E (17) (**Supplementary Figure 4**), supporting the existence of 5'
250 ORF1a RNAs in other coronaviruses. All together, these data support the hypothesis
251 that subgenomic RNAs containing just the 5' region of ORF1a are produced by SARS-
252 CoV-2.
253
254 **Junctions have the potential to generate variant open reading frames.**
255 To test the hypothesis that non-canonical junctions can result in variant open reading
256 frames (ORFs) in nc-sgRNAs, we assessed the ORF content of each read in the three
257 dRNAseq transcriptomes. Because dRNAseq can have an error rate of greater than
258 10% (18), we generated "coordinate-derived transcripts" by determining the start, end,
259 and junction coordinates of each raw transcript by mapping to SARS-CoV-2
260 (NC_045512.2) and extracting the associated genomic sequence. While this approach
261 is capable of overcoming sequencing errors and can resolve major RNA species, it is
262 not capable of resolving small or structurally complex RNA rearrangements. Because
263 the 5' end of nanopore reads may be truncated due to technical factors during

264 sequencing (19), we leveraged the assumption that functional sgRNAs should contain
265 the 5' leader sequence to identify reads generated from complete transcripts. While
266 excluding reads that don't contain the leader sequence may have reduced sensitivity, it
267 prevents identification of variant ORFs as a consequence of truncated reads.
268
269 ORFs were predicted directly from the coordinate-derived transcripts, and ORFs of
270 unexpected length were identified as "variant". Assessment of the relative abundance of
271 variant and canonical ORFs revealed evidence of variant ORFs of ORF1a/b, S, and M
272 (**Figure 6A**).
273
274 To characterize the identified M, S, and ORF1a ORF variants, we determined the stop
275 and start points of each ORF variant relative to their canonical counterparts (**Figure 6D-**
276 **L**). This analysis revealed that all theoretical M ORF variants were predicted to start at a
277 UUG start codon 42 amino acids before the end of the M gene and end at the canonical
278 stop codon (**Figure 6D, G, J**). M ORF variants make up between 7.9% and 19% of M
279 ORFs in the three dRNAseq datasets and are generated by the major junction point at
280 the ORF6 TRS sequence within the M reading frame (**Figure 1D-F**). If translated, M
281 ORF variants would lack the N-terminal transmembrane domains and contain regions
282 predicted to be present on the inside of the virion or in the cytosol. While the efficacy of
283 translation initiation from this start codon is unknown, it has an acceptable Kozak
284 consensus site with an A at the -3 position.
285

286 S ORF variants make up between 5.1% and 24.2% of all S ORFs identified in these
287 datasets (**Figure 6A-C**). The majority of S ORF variants are predicted from nc-sgRNAs
288 with 3' junctions landing within the S ORF (**Supplementary Figure 2D-F**), resulting in
289 N-terminal truncations with theoretical AUG and non-AUG start codons (**Figure 6E, H,**
290 **K**). If translated, these variants would lack the N-terminal signal sequence (20) and,
291 especially considering the variations in ORF start sites, it is unclear if these ORFs
292 encode functional isoforms.
293
294 Our identification of ORF1a variants is consistent with the observed patterns of 5'
295 ORF1a coverage (**Figure 5**). The peak end position of identified ORF1a variant ORFs is
296 around amino acid position 500 (**Figure 6F, I, L**), consistent with the observed decrease
297 in read coverage around genome position 1600. This position falls within the NSP2
298 amino acid sequence suggesting that, if translated, many ORF1a ORF variants would
299 consist of NSP1 and N-terminal fragments of NSP2. Interestingly, we found that
300 approximately 1/3 of ORF1a variants are in-frame fusions with downstream ORFs,
301 encoding mostly N (**Figure 6M-O**).
302

303 Discussion

304 While prior studies have identified nc-sgRNAs in SARS-CoV-2 (8, 11) and other
305 coronaviruses (17), there has been no comprehensive analysis of SARS-CoV-2 nc-
306 sgRNAs. We conducted an integrative analysis of eight independent SARS-CoV-2
307 transcriptomes to catalogue unexpected, non-canonical RNA species. We show that
308 SARS-CoV-2 produces nc-sgRNAs, that these nc-sgRNAs increase in abundance over

309 time, and that they are not associated with TRS-like homology. We highlight strong
310 evidence supporting the existence of nc-sgRNAs containing only the 5' region of ORF1a
311 and show that the presence of nc-sgRNAs can alter the landscape of viral ORFs.
312
313 We found that canonical sgRNAs are consistently produced across SARS-CoV-2
314 transcriptomes, and identify eight major sgRNAs encoding S, ORF3a, E, M, ORF6,
315 ORF7a/b, ORF8, and N. Each of these sgRNAs is supported by abundant 3' junctions
316 originating at a TRS-B just upstream the associated ORF. Similar to other reports, we
317 do not find evidence of a major series of sgRNAs encoding ORF10 (7, 8, 11). We also
318 do not find strong evidence of a major group of sgRNAs encoding ORF7B despite the
319 presence of a TRS-core-like sequence (A**A**GAAC) proximal to the ORF7B start.
320
321 Interestingly, up to 33% of sgRNAs from infected cells *in vitro* are non-canonical. One
322 potential source of nc-sgRNAs are DVGs introduced by defective particles during
323 infection. These can accumulate during the propagation of virus stocks. While
324 information on the passaging of viral stocks is only available for four transcriptomes, at
325 least five of the six SARS-CoV-2 transcriptomes generated from cell lines were
326 generated following a low MOI infection, which may reduce the impact of defective
327 particles (21, 22). Indeed, while there is some variation in the absolute abundance of
328 non-canonical junctions across transcriptomes that may reflect dataset-specific factors,
329 the relative abundance of non-canonical junctions at most genomic positions is
330 generally similar. One exception is that dataset-specific junctions are found in the Finkel
331 et al. transcriptomes. In particular, there is a strong 5' junction point at position 16971

332 that represents over 12% of non-canonical junctions in two Finkel et al. replicates but is
333 largely absent in other transcriptomes. A hypothesis that could explain this observation
334 is that there is a population of defective particles in the Finkel et al. virion preparation
335 that contain an internal deletion. This DVG, which is smaller than the full genome, may
336 have a replicative advantage during virus stock preparation (16). Indeed, the Finkel et
337 al.-specific junction at 16971 displays a relatively large increase in abundance over
338 time, in contrast to smaller and non-specific increases of non-canonical junctions at
339 other positions.
340
341 The consistent presence of non-canonical junctions across the SARS-CoV-2 genome in
342 independent transcriptomes suggests that the bulk of the observed nc-sgRNAs are not
343 dataset-specific but are generalizable to SARS-CoV-2 biology. Furthermore, their
344 nonspecific increase in abundance over time *in vitro* supports a model in which nc-
345 sgRNAs are generated nonspecifically and at higher frequencies later in infection. We
346 found that non-canonical junctions are not associated with TRS-like homology, raising
347 the possibility that there is another mechanism behind their formation. For example, it is
348 possible that factors such as RNA structure (23), accumulation of viral proteins, or
349 actions of the viral RdRp and associated cofactors (24) could influence nc-sgRNA
350 formation. Indeed, a recent study of the murine betacoronavirus MHV suggests that the
351 3'-to'5' exoribonuclease Nsp14 influences recombination site selection of the viral RdRp
352 (24). Additional studies are necessary to gain a mechanistic understanding of the
353 factors that influence nc-sgRNA generation and to understand the phenotypic effects of
354 nc-sgRNAs on SARS-CoV-2 pathogenesis. Notably, considering that defective viral

355 genomes in negative-sense RNA viruses have been associated with antiviral immunity,
356 dendritic cell maturation, and interferon production (5, 16, 25, 26) it will be important to
357 assess if SARS-CoV-2 nc-sgRNAs are associated with immune activity.
358
359 Junctions in viral RNA change the landscape of viral ORFs. Because the ORF6 TRS-B
360 is located 151 bases into the M ORF, sgRNAs created using this TRS-B contain a 3'
361 region of M. There is a UUG located 41 codons prior to the end of M that will now be
362 situated prior to the ORF6 on these sgRNAs. While UUG is a relatively weak start
363 codon, there is potential that this UUG could stimulate translation of a C-terminal M
364 fragment or regulate the expression of the downstream ORF6 as an upstream ORF
365 (27). Additional studies are needed to understand if this M ORF variant is translated and
366 to understand if its UUG start codon influences ORF6 translation.
367
368 In addition to this M ORF variant, we found that some nc-sgRNAs contain S and ORF1a
369 ORF variants. Many of the S ORF variants would lack the N-terminal signal sequence
370 (28) and, especially considering the variation in the hypothetical start positions of these
371 variants, it is unclear if they are translated. Notably, subgenomic RNAs encoding variant
372 S ORFs have been reported for SARS-CoV-1 (29).
373
374 In contrast, the ORF1a ORF variants have a peak stop position around ORF1a amino
375 acid position 500, which correlates well with an observed decrease in ORF1a 5'
376 coverage around genome position 1600. There is strong support for the existence of 5'
377 ORF1a-containing nc-sgRNAs across all eight transcriptomes studied here. Although

there isn't a strong peak of 5' junctions at specific positions in the 5' region of ORF1a, the consistent decreases in coverage and concomitant increases in 5' junctions around positions 1600 and 6000 are notable. It is possible that there are biological factors at these positions that mediate these generalized inflection points but, unlike TRS-mediated homology, don't concentrate junctions to a specific base. As posited by Kim et al. (8), the existence of subgenomic RNAs with the 5' end of ORF1a raises the possibility that these nc-sgRNAs may influence the relative abundance of Nsps, making this observation an important target for future study.

Conclusions

In conclusion, we show that SARS-CoV-2 generates nc-sgRNAs *in vitro* and *in vivo*, and that these nc-sgRNAs are largely consistent across independent transcriptomes. We show that nc-sgRNAs are not associated with TRS-like homology, suggesting there may be a homology-independent mechanism driving their formation. Finally, we show that non-canonical junctions have the potential to influence the landscape of viral ORFs, and that there is especially strong support for nc-sgRNAs that contain only a 5' portion of ORF1a. Future studies are necessary to understand the mechanisms behind nc-sgRNA formation, and to understand the influence of nc-sgRNAs on SARS-CoV-2 pathogenesis.

Materials and Methods

Sequencing data

401 Details on all studied transcriptomes are listed in the table below:

Source	**Virus Isolate (MOI)** **(Details on stock generation)**	**Infection host**	**Timepoint**	**Accession or DOI**	**Technology**
Taiaroa et al. (7)	Australia/VIC01/2020 (MOI: Unknown) (Passage unknown)	Vero cells	Unknown	SRR11350376	dRNAseq
Kim et al. (8)	Korea/KCDC02/2020 (MOI: 0.05) (4th passage. No plaque isolation)	Vero cells	24hpi	10.17605/OSF.IO/8F6N9	dRNAseq
Davidson et al. (9)	England/VE6-T/2020 (MOI: Unknown) (2nd passage. No plaque isolation).	Vero cells	Unknown	10.5281/zenodo.3722580	dRNAseq
Finkel et al. (12)	GISAID Acc. No. EPI_ISL_406862 (MOI: 0.2) (4th passage. No plaque isolation.)	Vero cells	5hpi	SRR11713354	Illumina PolyA
Finkel et al. (12)	GISAID Acc. No. EPI_ISL_406862 (MOI: 0.2) (4th passage. No plaque isolation.)	Vero cells	24hpi	SRR11713362	Illumina PolyA
Blanco-Melo et al. (13)	USA/WA1/2020 (MOI: 0.2) (Passage unknown)	A549-ACE2 cells	24hpi	SRR11517741	Illumina PolyA
Blanco-Melo et al. (13)	USA/WA1/2020 ($5*10^4$ PFU/ferret) (Passage unknown)	Ferret (Nasal washings)	3dpi	SRR11517855-SRR11517858	Illumina PolyA
Suzuki et al. (15)	SARS-CoV-2/Hu/DP/Kng/19-020 ($5*10^4$ PFU/100 organoids) (Passage unknown but **plaque isolated**)	Bronchial organoids	5dpi	SRR11811022	Illumina PolyA
Emanuel et al. (14)	Frankfurt strain AY310120.1 **OR** BetaCoV/Munich/BavPat1/2020|EPI_ISL_406862 (MOI: 0.33) (Passage unknown)	Calu3	4hpi	SRR11550047	Illumina Total RNA
Emanuel et al. (14)	Frankfurl strain AY310120.1 **OR** BetaCoV/Munich/BavPat1/2020|EPI_ISL_406862 (MOI: 0.33) (Passage unknown)	Calu3	24hpi	SRR11550045	Illumina Total RNA

Viehweger et al. (17)	CoV-229E (MOI: 3) (Passage unknown)	Huh7 cells	24hpi	ERR3460961	dRNAseq

Hpi: Hours post infection

Dpi: Days post infection

In the case of the Finkel et al. and Emanual et al. transcriptomes, the 24hpi samples were used in all analyses except for the investigation of junction changes over time.

Determining junction coordinates.

Reads in all transcriptomes were mapped against the SARS-CoV-2 reference genome (accession NC_045512.2) using minimap2 (30) and custom parameters detailed in minimap_sars2.sh and inspired by Kim et al. (8), and unmapped reads were discarded. The exceptions are the transcriptomes from Finkel et al. and Emanuel et al. – because their read lengths were very short (60 and 72 bases in length respectively), mapping was conducted with STAR (31) using settings detailed in star.sh.

The 5' and 3' junction positions of junction-spanning reads were determined with generate_synthetic_transcripts.py. This script reads a BAM file and the SARS-CoV-2 genome fasta and, by parsing the BAM alignment CIGAR and start position, determines the start, end, and junction coordinates of the alignment. Any minimap2-called deletion or intron of at least 1000 bases in length was considered a junction. Junction coordinates were then written to a tab-delimited output file for further analysis.

Analysis and visualization of junctions.

424 The 5’ and 3’ coordinates of each junction were processed in R (32), and figures
425 generated with ggplot2 (33). Gene-maps were generated using the gggenes R package
426 (34).
427
428 For the global distribution of reads in each transcriptome (**Figure 1A-C,**
429 **Supplementary Figure 1A-F**), specific 5’-3’ junctions that occur at least twice are
430 represented as arcs. Each inverted peak represents a histogram of 5’ or 3’ junctions at
431 each genome position, with a bin size of 100 bases – this means that the magnitude of
432 each peak represents the total number of 5’ or 3’ junctions within each 100 base span.
433 Code: global_junctions.Rmd
434
435 The distribution of major 3’ junctions (**Figure 1D-F**) was generated by plotting a
436 histogram of 3’ junction positions that occur after position 21000 and that have a 5’ end
437 prior to position 100. Bin-size is 20 bases. Code: canonical_3prime_junctions.Rmd
438
439 The percentage of non-canonical junctions in each transcriptome (**Figure 2A,**
440 **Supplementary Figure 1G**) was calculated by first assigning each individual 5’-3’
441 junction as canonical or non-canonical. A junction was considered to be canonical if it’s
442 5’ position was within 20 bases of the TRS-L core sequence ACGAAC (starting at
443 position 69), and it’s 3’ junction was within 15 bases of a TRS-B (defined by the
444 presence of the TRS core sequence). The percentage of total junctions that were
445 assigned as non-canonical was then determined. Code: global_junctions.Rmd
446

447 **Identifying dataset-specific junctions (Figure 2).**

448 The consistency of non-canonical junctions across transcriptomes (**Figure 2C, D**) was
449 determined separately for 5' and 3' junctions based on one replicate each from Taiaroa
450 et al., Kim et al., Davidson et al., Finkel et al., and Blanco-Melo et al. transcriptomes
451 generated from cells infected with SARS-CoV-2 *in vitro*. For each SARS-CoV-2 genome
452 position, the percentage of non-canonical junctions at that site was calculated for each
453 transcriptome (X). The mean (μ) and standard deviation (σ) of percentages at each site
454 across the five transcriptomes were then calculated. For each position in each
455 transcriptome, a z-score was calculated by subtracting the observed percentage by the
456 mean and dividing by the standard deviation ((X-μ)/σ). This process is visualized in
457 **Figure 2B**. Code: dataset_specific_junctions.Rmd

458

459 **Change in junctions over time** (**Figure 3**).

460 The change in junctions over time was determined based on datasets from Finkel et al.
461 (5hpi and 24hpi) and Emanuel et al. (4hpi and 24hpi). The percentage of junctions that
462 originate at each genome position was determined for each timepoint, and the absolute
463 difference between the two values was calculated. Notably, this analysis (**Figure 3B, C**)
464 focused on 5' and 3' counts at each position separately, such that a percentage of 5'
465 junctions and a percentage of 3' junctions at each position was determined. To
466 determine the aggregated change in each <u>class</u> of junctions (**Figure 3F,G**), each 5'-3'
467 junction was assigned to a class based on the location of its 5' and 3' position. If a
468 junction's 5' position was located within 20 bases of the TRS-L, and it's 3' position was
469 located within 15 bases of a TRS-B, it was assigned to the ORF closest to the TRS-B.

470 Otherwise, the junction was assigned as non-canonical. The percentage of total
471 junctions in each class at the early timepoint was subtracted from the class percentages
472 at the late timepoint for each dataset. Code: junctions_over_time.Rmd
473
474 **Assessing homology near 5' and 3' positions of each junction** (**Figure 4**).
475 The identity and length of homologous sequences flanking the 5' and 3' sites of each
476 junction were determined by identifying the 30 bases flanking each junction site. The
477 longest identical subsequence between these two 30 base sequences was then
478 collected. For **Figure 4B-D**, the most common homology sequence was plotted for each
479 group of junctions. Here, a junction was considered canonical if it has a 3' end within 15
480 bases of a canonical TRS-B or was assigned as "Within ORF" if it was otherwise within
481 an ORF. The exception were junctions with a 5' end within ORF1a – these were
482 assigned to ORF1a. The total distribution of homology lengths was also determined for
483 canonical and non-canonical junctions (**Figure 4E-G**). To determine the random
484 distribution of homology lengths, all 30 base sequences (30mers) present in the SARS-
485 CoV-2 genome were determined. The longest identical subsequence between 100,000
486 random pairs of 30mers that are derived from at least 1000 bases apart on the genome
487 was determined. Code: TRS_plotting.Rmd
488
489 **Assessment of excess 5' ORF1a genome coverage (Figure 5).**
490 Coverage at each position was assessed from SARS-CoV-2-mapped BAMs using the
491 depth subcommand of samtools (35). (Command:

492 samtools depth -aa -d0 file.bam > file.cov). Coverage and cumulative number of 5'
493 junctions (excluding junctions occurring before position 100) were plotted. Code:
494 ORF1a_coverage.Rmd
495
496 **Analysis of ORFs on dRNAseq reads (Figure 6).**
497 generate_synthetic_transcripts.py was used to generate "coordinate-derived transcripts"
498 from the SARS-CoV-2 mapped BAMs from the Taiaroa et al., Kim et al., and Davidson
499 et al. dRNAseq transcriptomes. This script reads a BAM file and the SARS-CoV-2
500 genome fasta and, by parsing the BAM alignment CIGAR and start position, determines
501 the start, end, and junction coordinates of the alignment. Coordinate-derived transcripts
502 were created by using these coordinates to retrieve the associated sequence from the
503 SARS-CoV-2 genome. Any minimap2-called deletion or intron of at least 1000 bases in
504 length was considered a junction. All coordinate-derived transcripts were then aligned
505 against a minimal leader sequence fragment (5' –
506 CTTCCCAGGTAACAAACCAACCAACTTTCGATCTCTTGTAGATCTGTTCTC – 3')
507 using blastn (36). This minimal sequence was used instead of the full leader sequence
508 because inspection of 5' coverage in the three long-read datasets revealed a significant
509 drop in coverage at the end of this sequence. Transcripts with an alignment of at least
510 45 nucleotides in length and a percent identity of at least 85%, and that contain the start
511 of this sequence within the first 50 nucleotides of the transcript, were kept. Transcripts
512 not containing this leader sequence were discarded.
513

514 ORFs were called directly from each transcript using Prodigal (37), using parameters
515 listed in prodigal.sh. ORFs were allowed to initiate from any nUG start codon, were not
516 required to be the most 5' ORF on each transcript and were only reported if they are at
517 least 30 codons in length. Each ORF was translated into amino acid sequence using
518 prodigal_to_orf_direct.py. If multiple Prodigal-predicted ORFs contained an overlapping
519 amino acid sequence, the longest ORF was output. Each ORF was output in fasta
520 format and labeled with transcript of origin and coordinates of the ORF on the transcript.
521
522 The amino acid sequence of each ORF was then mapped against canonical SARS-
523 CoV-2 proteins (from accession NC_045512.2) as well as Prodigal-predicted
524 unannotated ORFs from the SARS-CoV-2 genome using DIAMOND (38). DIAMOND
525 parameters are described in diamond.sh and include an E-value threshold of 10. During
526 downstream analysis, alignments were considered valid if the aligned portions
527 maintained at least 95% amino acid identity to the reference protein.
528
529 Various statistics of each ORF, including alignment information, the start position of the
530 ORF on the transcript, and fusion information, were generated from the DIAMOND
531 alignment file using parse_orf_assignments.py. An ORF was considered variant if it was
532 not the same length as the canonical protein, with a notable exception. Because there
533 are alternative start codons upstream of some annotated genes, and Prodigal would call
534 ORFs using these start codons if they are present on a transcript, ORFs were allowed
535 to have up to 20 amino acids of additional N-terminal amino acids while still being
536 classified as canonical if they end at the expected position. If an ORF had matches

537 against multiple SARS-CoV-2 proteins, it was given a primary assignment of the protein

538 with the longest alignment length.

539

540 **Code availability**

541 The reproducible computational pipeline used to generate all results is publicly available

542 at https://github.com/jnoms/virORF_direct.

543

544 List of abbreviations

545 CoV: Coronavirus

546 dRNAseq: Direct RNA sequencing

547 E: Envelope protein

548 M: Matrix protein

549 N: Nucleocapsid protein

550 Nsp: Nonstructural protein

551 ORF: Open reading frame

552 S: Spike protein

553 SARS-CoV-2: Systemic acute respiratory syndrome Coronavirus 2

554 TRS: Transcriptional regulatory sequence

555

556 Declarations

557

558 **Ethics approval and consent to participate**: Not applicable

559

560 **Consent for publication**: Not applicable

561

562 **Availability of data and materials**: Code is available in the virORF_direct repository,

563 https://github.com/jnoms/virORF_direct.

564

565 **Competing interests**

566 M.M. receives research support from Bayer, Ono, and Janssen, has patents licensed to

567 Bayer and Labcorp, and is a consultant for OrigiMed. J.A.D. received research support

568 from Constellation Pharmaceuticals and is a consultant for EMD Serono, Inc. and Merck

569 & Co. Inc.

570

571 **Funding**

572 This work was supported in part by the US Public Health Service grants R35CA232128

573 and P01CA203655 to J.A.D.

574

575 **Authors' Contributions**

576 J.N. analyzed the data; J.N., M.M., J.A.D. designed the study and wrote the manuscript.

577

578 **Acknowledgements**

579 The authors thank Taiaroa et al., Kim et al., Davidson et al., Blanco-Melo et al., Suzuki

580 et al., Finkel et al., and Emanuel et al. for collecting the RNA sequencing data and

581 making these data publicly available. Portions of this research were conducted by using

582 the O2 High Performance Compute Cluster, supported by the Research Computing
583 Group at Harvard Medical School.
584

585 # Figure legends

586

587 **Figure 1. SARS-CoV-2 generates a defined population of canonical subgenomic**
588 **RNAs.**

589 **A-C)** For each location on the viral genome, a histogram of 5' and 3' junctions at that
590 position was calculated and plotted as an inverse peak. The histogram bin size is
591 100 bases, meaning each inverse peak represents the cumulative count of 5' or 3'
592 junctions occurring within that span. Curved lines represent the 5' and 3' locations of
593 junctions that occur at least twice. Red curves represent canonical junctions, black
594 curves represent non-canonical junctions. "Taiaroa" (7), "Kim" (8), and "Davidson"
595 (9) represent the three independent SARS-CoV-2 dRNAseq datasets investigated.
596 **D-F)** A histogram of 3' junctions past position 21000 with a 5' end before position
597 100 are plotted. Dashed lines indicate the start coordinates of annotated viral genes.
598 Bin-size is 20 bases.
599 **G)** Based on junction analysis, the predicted major species of virus-produced RNAs
600 are represented. The most 5' gene or genes on each subgenomic RNA is listed.

601

602 **Figure 2. Non-canonical junctions are consistent across independent datasets.**

603 **A)** Percentage of junctions that are non-canonical in five independent datasets.
604 Junctions were assigned as canonical if their 5' location was within 20 bases of

605 the TRS-L and their 3' location within 15 bases of a TRS-B, and otherwise
606 assigned as non-canonical. Taiaroa, Kim, and Davidson are dRNAseq, while
607 Finkel and Blanco-Melo are Illumina PolyA RNAseq.
608 **B)** Illustration of computational approach to determine the consistency of 5' and
609 3' junction points across independent datasets. The percentage of non-canonical
610 junctions at each genome position in each dataset was determined (X). The
611 mean (μ) and standard deviation (σ) of percentages at each position across the
612 five datasets was calculated. For each position in each dataset, the Z-score was
613 calculated as (X-μ)/σ (i.e. the number of standard deviations away from the
614 mean), and the percentages and Z-scores for each position in each dataset were
615 plotted.
616 **C, D)** Each point represents the percentage and Z-score of one position in one
617 dataset. For each position in the SARS-CoV-2 genome, the percentage and Z-
618 score of non-canonical junctions with a 5' end (D) or a 3' end (E) was determined
619 as described above for five independent datasets: Taiaroa, Kim, Davidson,
620 Finkel, and Blanco-Melo. Points with a percentage above 4% of non-canonical
621 junctions and a Z-score above 1 were highlighted.
622
623 **Figure 3. Non-canonical junctions accumulate over time *in vitro*.**
624 **A)** Illustration of computational approach used to determine change in junction
625 percentages over time. For each position in the SARS-CoV-2 genome and
626 separately for 5' and 3' junctions, the number of junctions at that position was
627 calculated. Using these numbers, the percentage of 5' or 3' junctions falling at

628 each position was calculated. The change in junction percentage at each position
629 is defined as the difference between the position's junction percentage at the late
630 and early timepoints, and this junction change was plotted for each position.
631 **B-E)** The change in junction percentage for 5' (orange) and 3' (blue) junctions
632 over time in the Finkel (B, D) and Emanuel (C, E) datasets was determined as
633 described above. Changes in the percentage of junctions Positions with at
634 change greater than 2.5% are annotated with text on the plot. Panels D and E
635 are zoomed in versions of B and C.
636 **F, G)** Junctions were assigned into groups based on their 5' and 3' junction
637 positions. If a junction had a 5' end within 20 bases of the TRS-L and within 15
638 bases of a TRS-B, it was considered a canonical junction belonging to the ORF
639 with a start closest to the TRS-B. Otherwise, it was considered non-canonical.
640 The percentage of junctions falling into each category was calculated for early
641 and late timepoints, and the difference between each category's percentage in
642 the late vs early timepoint was plotted.
643
644 **Figure 4. Non-canonical junctions are not associated with TRS-like homology.**
645 **A)** Illustration of computational approach used to assess homologous sequences
646 between the 5' and 3' junction points. For each of the three dRNAseq datasets,
647 the 30 bases flanking the 5' and 3' junction points were assessed, and the
648 longest homologous sequence between these two 30 base regions was
649 determined.

650 **B-D)** Homologous sequences present in the 15 bases on either side of the 5' and
651 3' ends of each junction. Junctions are classified by the location of their 3' end –
652 if this is within 15 bases of the canonical TRS site or if it falls within a gene it is
653 assigned accordingly. The only exception is ORF1a – junctions with a 5' end
654 originating in ORF1a are assigned to ORF1a. Labels represent the most
655 common homologous sequence between the ends of each junction. The core
656 TRS sequence ACGAAC is underlined.
657 **E-G)** The length of the longest homologous sequence for canonical (C) and non-
658 canonical (NC) are plotted. Here, junctions were considered canonical if they
659 have a 5' end within 20 nucleotides of the TRS-L and a 3' end within 15
660 nucleotides of a TRS-B. (R) represents random homology lengths. The points for
661 (R) were calculated by first extracting all possible 30 base sequences (30mers)
662 from the SARS-CoV-2 genome, and then assessing the length of the longest
663 homologous sequence between 100,000 random pairs of 30mers that are
664 separated by at least 1000 bases on the genome. Within each column, the
665 relative width of each band represents the relative abundance of junctions with
666 each homology length. The value at the top of each column is the mean
667 homology length.
668
669 **Figure 5. Relative abundance of subgenomic RNAs that contain only the 5' end of**
670 **ORF1a.**

671 **A-H)** Read coverage (black) and cumulative 5' junctions (red) are plotted for
672 eight independent datasets. The sequencing strategy and sample types are
673 annotated.
674 **I)** A schematic of a representative subgenomic RNA that consists of only the 5'
675 region of ORF1a. Pileups showing reads can be found in Supplementary Figure
676 3.
677
678 **Figure 6. Junctions have the potential to generate variant open reading frames.**
679 **A-C)** ORFs were predicted directly from transcript-derived reads for the three
680 dRNAseq datasets. Each ORF was aligned against the protein sequences of
681 canonical SARS-CoV-2 genes using the DIAMOND aligner. Variant ORFs were
682 defined as ORFs that were assigned to a canonical SARS-CoV-2 protein but had
683 an unexpected start or stop position, while perfectly-aligning ORFs were
684 considered canonical. The percentage of canonical and variant ORFs for each
685 protein is plotted.
686 **D-L**) Schematics of M, N, and ORF1ab are displayed with the approximate
687 location of predicted transmembrane domains labeled in red. A histogram of the
688 start and end sites of variant M, N, and ORF1ab ORFs are displayed. Start sites
689 of each variant ORF are on top, and end sites are on the bottom of each panel.
690 Percentages represent the percentage of each ORF that is variant. Histogram
691 bin-sizes: M, 1; N, 10 ; ORF1ab, 20. NTD: N-terminal domain. RBD: Receptor
692 binding domain. CD: Connector domain. NSP: Nonstructural protein.

693 **M-O)** The identity of ORF1a-fusion partners is plotted on the Y axis, with the
694 count of such fusions on the X axis. The top 10 fusion partners for each sample
695 are represented. Color indicates if the fusion partner is on the N and C terminus
696 of ORF1a, if the terminus is ambiguous, or if the fusion is a "self" fusion between
697 an upstream and downstream region of ORF1a. The percentage notes the
698 percent of ORFs assigned to ORF1a that have a fusion.
699
700 **Supplementary Figure 1. There is evidence of non-canonical junctions in diverse**
701 **datasets.**
702 **A-E)** For each location on the viral genome, a histogram of 5' and 3' junctions at
703 that position was calculated and plotted as an inverse peak. The histogram bin
704 size is 100 bases, meaning each inverse peak represents the cumulative count
705 of 5' or 3' junctions occurring within that span. Curved lines represent the 5' and
706 3' locations of junctions that occur at least twice. Red curves represent canonical
707 junctions, black curves represent non-canonical junctions.
708 **F)** The percentage of junctions that are canonical in the Suzuki (Bronchial
709 organoids) and Blanco-Melo (Ferret) datasets was determined. Junctions were
710 assigned as canonical if their 5' location was within 20 bases of the TRS-L and
711 their 3' location within 15 bases of a TRS-B, and otherwise assigned as non-
712 canonical.
713
714 **Supplementary Figure 2. Dataset-specific junctions**

715 **A-E)** The percentage of non-canonical junctions at each SARS-CoV-2 genome
716 position is plotted. Plots A-C show the percentage of 5' junctions at each
717 position, while D-E show the percentage of 3' junctions at each position. The
718 plotted samples include three replicates from Blanco-Melo et al., Davidson et al,
719 two replicates from Finkel et al, and the Kim and Taiaroa et al datasets.
720

721 **Supplementary Figure 3. Subgenomic RNAs containing non-canonical junctions**
722 **are present in three independent dRNAseq datasets.**

723 **A-F)** Subgenomic RNAs with 5' junctions occurring in ORF1a (A-C) or 3'
724 junctions occurring in S (D-F) are plotted for the three dRNAseq datasets. Each
725 row is a read, and regions in black indicate the read contains that sequence.
726

727 **Supplementary Figure 4. There is elevated ORF1a coverage in CoV 229E.**

728 **A)** Read coverage (black) and cumulative 5' junctions (red) are plotted for
729 dRNAseq data from CoV 229E-infected cells.
730
731

732 # References

733 1. Wu F, Zhao S, Yu B, Chen Y-M, Wang W, Song Z-G, et al. A new coronavirus
734 associated with human respiratory disease in China. Nature. 2020;579(7798):265-9.
735 2. Plant EP, Dinman JD. The role of programmed-1 ribosomal frameshifting in
736 coronavirus propagation. Frontiers in bioscience: a journal and virtual library.
737 2008;13:4873.
738 3. Narayanan K, Huang C, Makino S. SARS coronavirus accessory proteins. Virus
739 research. 2008;133(1):113-21.
740 4. de Haan CA, Masters PS, Shen X, Weiss S, Rottier PJ. The group-specific
741 murine coronavirus genes are not essential, but their deletion, by reverse genetics, is
742 attenuating in the natural host. Virology. 2002;296(1):177-89.

5. Yount B, Roberts RS, Sims AC, Deming D, Frieman MB, Sparks J, et al. Severe acute respiratory syndrome coronavirus group-specific open reading frames encode nonessential functions for replication in cell cultures and mice. Journal of virology. 2005;79(23):14909-22.
6. Sawicki SG, Sawicki DL, Siddell SG. A contemporary view of coronavirus transcription. Journal of virology. 2007;81(1):20-9.
7. Taiaroa G, Rawlinson D, Featherstone L, Pitt M, Caly L, Druce J, et al. Direct RNA sequencing and early evolution of SARS-CoV-2. bioRxiv. 2020:2020.03.05.976167.
8. Kim D, Lee J-Y, Yang J-S, Kim JW, Kim VN, Chang H. The architecture of SARS-CoV-2 transcriptome. Cell. 2020.
9. Davidson AD, Williamson MK, Lewis S, Shoemark D, Carroll MW, Heesom KJ, et al. Characterisation of the transcriptome and proteome of SARS-CoV-2 reveals a cell passage induced in-frame deletion of the furin-like cleavage site from the spike glycoprotein. Genome Medicine. 2020;12(1):1-15.
10. Kim D, Lee J-Y, Yang J-S, Kim JW, Kim VN, Chang H. The architecture of SARS-CoV-2 transcriptome. bioRxiv. 2020:2020.03.12.988865.
11. Davidson AD, Williamson MK, Lewis S, Shoemark D, Carroll MW, Heesom K, et al. Characterisation of the transcriptome and proteome of SARS-CoV-2 using direct RNA sequencing and tandem mass spectrometry reveals evidence for a cell passage induced in-frame deletion in the spike glycoprotein that removes the furin-like cleavage site. bioRxiv. 2020:2020.03.22.002204.
12. Finkel Y, Mizrahi O, Nachshon A, Weingarten-Gabbay S, Yahalom-Ronen Y, Tamir H, et al. The coding capacity of SARS-CoV-2. bioRxiv. 2020:2020.05.07.082909.
13. Blanco-Melo D, Nilsson-Payant BE, Liu W-C, Uhl S, Hoagland D, Møller R, et al. Imbalanced host response to SARS-CoV-2 drives development of COVID-19. Cell. 2020.
14. Emanuel W, Kirstin M, Vedran F, Asija D, Theresa GL, Roberto A, et al. Bulk and single-cell gene expression profiling of SARS-CoV-2 infected human cell lines identifies molecular targets for therapeutic intervention. bioRxiv. 2020:2020.05.05.079194.
15. Suzuki T, Itoh Y, Sakai Y, Saito A, Okuzaki D, Motooka D, et al. Generation of human bronchial organoids for SARS-CoV-2 research. bioRxiv. 2020:2020.05.25.115600.
16. Genoyer E, López CB. The impact of defective viruses on infection and immunity. Annual review of virology. 2019;6:547-66.
17. Viehweger A, Krautwurst S, Lamkiewicz K, Madhugiri R, Ziebuhr J, Hölzer M, et al. Direct RNA nanopore sequencing of full-length coronavirus genomes provides novel insights into structural variants and enables modification analysis. Genome research. 2019;29(9):1545-54.
18. Rang FJ, Kloosterman WP, de Ridder J. From squiggle to basepair: computational approaches for improving nanopore sequencing read accuracy. Genome biology. 2018;19(1):90.
19. Workman RE, Tang AD, Tang PS, Jain M, Tyson JR, Razaghi R, et al. Nanopore native RNA sequencing of a human poly (A) transcriptome. Nature Methods. 2019;16(12):1297-305.

20. Bosch BJ, Martina BE, Van Der Zee R, Lepault J, Haijema BJ, Versluis C, et al. Severe acute respiratory syndrome coronavirus (SARS-CoV) infection inhibition using spike protein heptad repeat-derived peptides. Proceedings of the National Academy of Sciences. 2004;101(22):8455-60.
21. Thompson KAS, Yin J. Population dynamics of an RNA virus and its defective interfering particles in passage cultures. Virology journal. 2010;7(1):257.
22. Brooke CB. Biological activities of'noninfectious' influenza A virus particles. Future virology. 2014;9(1):41-51.
23. Lan TCT, Allan MF, Malsick LE, Khandwala S, Nyeo SSY, Bathe M, et al. Structure of the full SARS-CoV-2 RNA genome in infected cells. bioRxiv. 2020:2020.06.29.178343.
24. Gribble J, Pruijssers AJ, Agostini ML, Anderson-Daniels J, Chappell JD, Lu X, et al. The coronavirus proofreading exoribonuclease mediates extensive viral recombination. bioRxiv. 2020:2020.04.23.057786.
25. Sun Y, Jain D, Koziol-White CJ, Genoyer E, Gilbert M, Tapia K, et al. Immunostimulatory defective viral genomes from respiratory syncytial virus promote a strong innate antiviral response during infection in mice and humans. PLoS Pathog. 2015;11(9):e1005122.
26. Strahle L, Garcin D, Kolakofsky D. Sendai virus defective-interfering genomes and the activation of interferon-beta. Virology. 2006;351(1):101-11.
27. Barbosa C, Peixeiro I, Romão L. Gene expression regulation by upstream open reading frames and human disease. PLoS Genet. 2013;9(8):e1003529.
28. Wrapp D, Wang N, Corbett KS, Goldsmith JA, Hsieh C-L, Abiona O, et al. Cryo-EM structure of the 2019-nCoV spike in the prefusion conformation. Science. 2020;367(6483):1260-3.
29. Hussain S, Chen Y, Yang Y, Xu J, Peng Y, Wu Y, et al. Identification of novel subgenomic RNAs and noncanonical transcription initiation signals of severe acute respiratory syndrome coronavirus. Journal of virology. 2005;79(9):5288-95.
30. Li H. Minimap2: pairwise alignment for nucleotide sequences. Bioinformatics. 2018;34(18):3094-100.
31. Dobin A, Davis CA, Schlesinger F, Drenkow J, Zaleski C, Jha S, et al. STAR: ultrafast universal RNA-seq aligner. Bioinformatics. 2013;29(1):15-21.
32. Team RC. R: A language and environment for statistical computing. 2013.
33. Wickham H. ggplot2. Wiley Interdisciplinary Reviews: Computational Statistics. 2011;3(2):180-5.
34. Wilkins D. gggenes: draw gene arrow maps in ‘ggplot2’. R package version 0.4. 0. 2019.
35. Li H, Handsaker B, Wysoker A, Fennell T, Ruan J, Homer N, et al. The sequence alignment/map format and SAMtools. Bioinformatics. 2009;25(16):2078-9.
36. Camacho C, Coulouris G, Avagyan V, Ma N, Papadopoulos J, Bealer K, et al. BLAST+: architecture and applications. BMC bioinformatics. 2009;10(1):421.
37. Hyatt D, Chen G-L, LoCascio PF, Land ML, Larimer FW, Hauser LJ. Prodigal: prokaryotic gene recognition and translation initiation site identification. BMC bioinformatics. 2010;11(1):119.
38. Buchfink B, Xie C, Huson DH. Fast and sensitive protein alignment using DIAMOND. Nature methods. 2015;12(1):59.

834

Figure 1

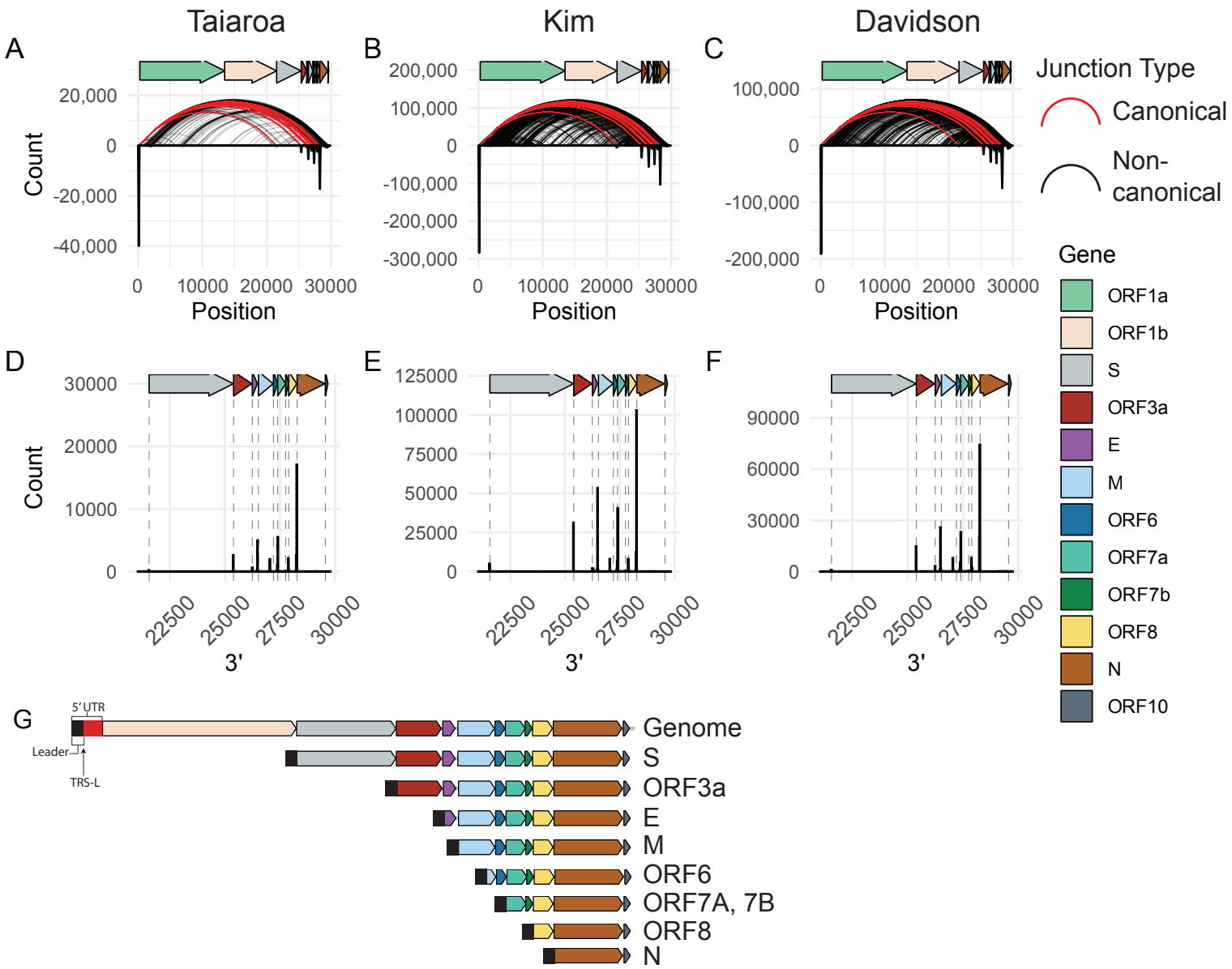

Figure 1. SARS-CoV-2 generates a defined population of canonical subgenomic RNAs.

A-C) For each location on the viral genome, a histogram of 5' and 3' junctions at that position was calculated and plotted as an inverse peak. The histogram bin size is 100 bases, meaning each inverse peak represents the cumulative count of 5' or 3' junctions occurring within that span. Curved lines represent the 5' and 3' locations of junctions that occur at least twice. Red curves represent canonical junctions, black curves represent non-canonical junctions. "Taiaroa", "Kim", and "Davidson" represent the three independent SARS-CoV-2 dRNAseq datasets investigated.

D-E) A histogram of 3' junctions past position 21000 with a 5' end before position 100 are plotted. Dashed lines indicate the start coordinates of annotated viral genes. Bin-size is 20 bases

G) Based on junction analysis, the predicted major species of virus-produced RNAs are represented. The most 5' gene or genes on each subgenomic RNA islisted.

Figure 2

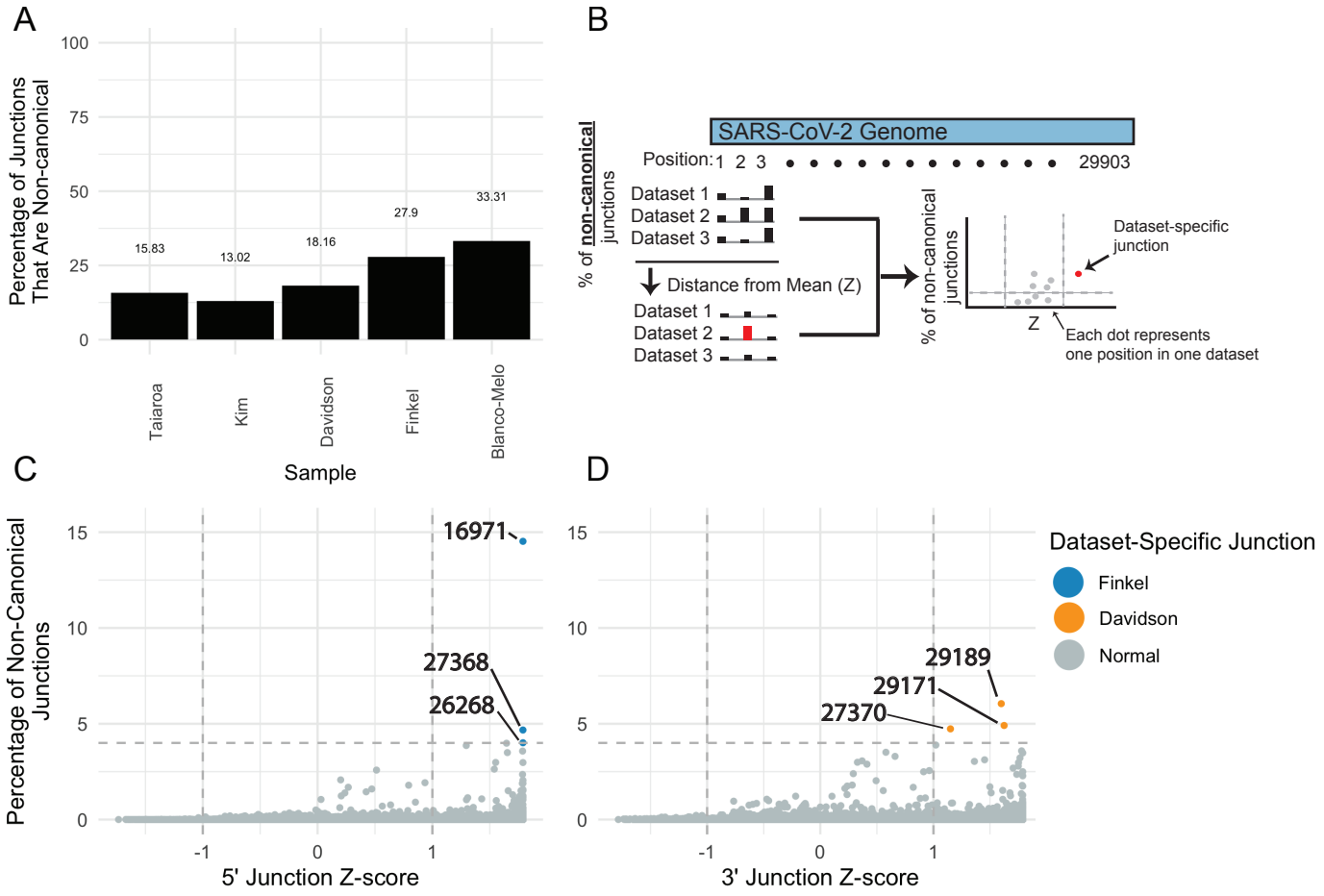

Figure 2. Non-canonical junctions are consistent across independent datasets.

A) Percentage of junctions that are non-canonical in five independent datasets. Junctions were assigned as canonical if their 5' location was within 20 bases of the TRS-L and their 3' location within 15 bases of a TRS-B, and otherwise assigned as non-canonical. Taiaroa, Kim, and Davidson are dRNAseq, while Finkel and Blanco-Melo are Illumina PolyA RNAseq.

B) Description of computational approach to determine the consistency of 5' and 3' junction points across independent datasets. The percentage of non-canonical junctions at each genome position in each dataset was determined (X). The mean (μ) and standard deviation (σ) of percentages at each position across the five datasets was calculated. For each position in each dataset, the Z-score was calculated as (X-μ)/σ (i.e. the number of standard deviations away from the mean), and the percentages and Z-scores for each position in each dataset were plotted.

C, D) Each point represents the percentage and Z-score of one position in one dataset. For each position in the SARS-CoV-2 genome, the percentage and Z-score of non-canonical junctions with a 5' end (D) or a 3' end (E) was determined as described above for five independent datasets: Taiaroa, Kim, Davidson, Finkel, and Blanco-Melo. Points with a percentage above 4% of non-canonical junctions and a Z-score above 1 were highlighted.

Figure 3

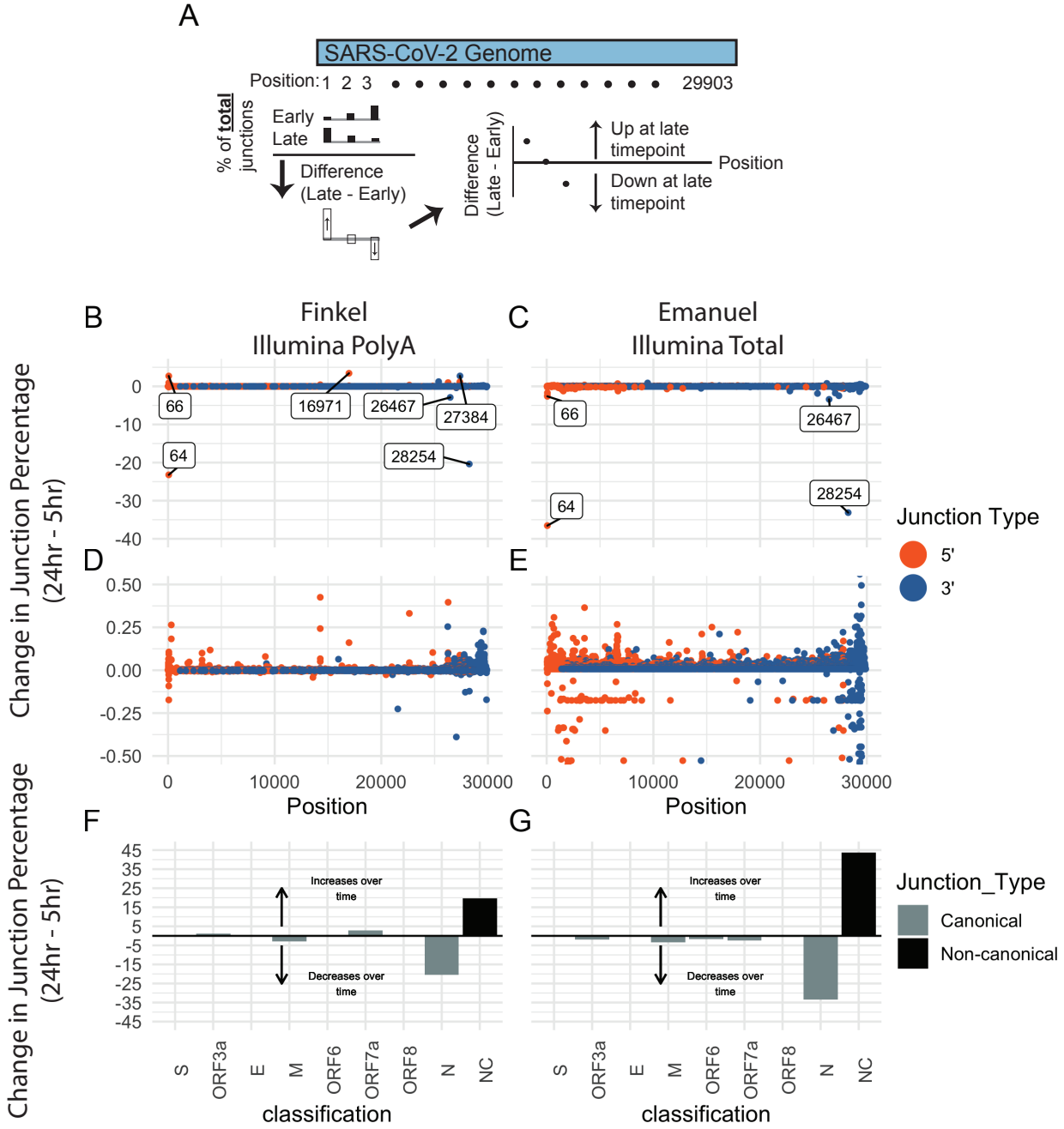

Figure 3. Non-canonical junctions accumulate over time in vitro.

A) Description of computational approach used to determine change in junction percentages over time. For each position in the SARS-CoV-2 genome and separately for 5' and 3' junctions, the number of junctions at that position was calculated. Using these numbers, the percentage of 5' or 3' junctions falling at each position was calculated. The change in junction percentage at each position is defined as the difference between the position's junction percentage at the late and early timepoints, and this junction change was plotted for each position.

B-E) The change in junction percentage for 5' (orange) and 3' (blue) junctions over time in the Finkel (B, D) and Emanuel (C, E) datasets was determined as described above. Changes in the percentage of junctions Positions with at change greater than 2.5% are annotated with text on the plot. Figures D and E are zoomed in versions of A and B.

F, G) Junctions were assigned into groups based on their 5' and 3' junction positions. If a junction had a 5' end within 20 bases of the TRS-L and within 15 bases of a TRS-B, it was considered a canonical junction belonging to the ORF with a start closest to the TRS-B. Otherwise, it was considered non-canonical. The percentage of junctions falling into each category was calculated for early and late timepoints, and the difference between each category's percentage in the late vs early timepoint was plotted.

Figure 4

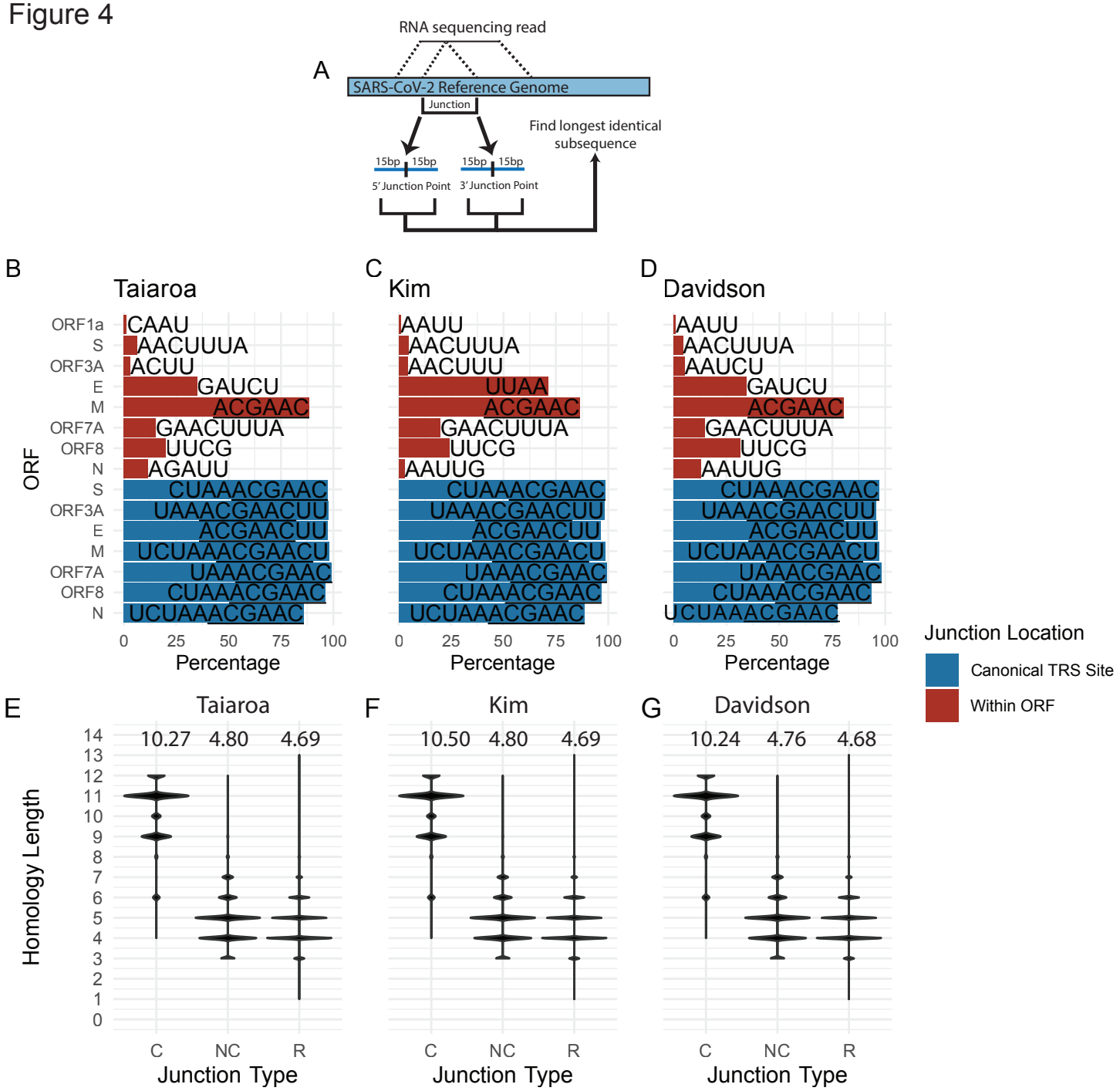

Figure 4. Non-canonical junctions are not associated with TRS-like homology.

A) Description of computational approach used to assess homologous sequences between the 5' and 3' junction points. For each of the three dRNAseq datasets, the 30 bases flanking the 5' and 3' junction points were assessed, and the longest homologous sequence between these two 30 base regions was determined.

B-D) Homologous sequences present in the 15 bases on either side of the 5' and 3' ends of each junction. Junctions are classified by the location of their 3' end – if this is within 15 bases of the canonical TRS site or if it falls within a gene it is assigned accordingly. The only exception is ORF1a – junctions with a 5' end originating in ORF1a are assigned to ORF1a. Labels represent the most common homologous sequence between the ends of each junction. The core TRS sequence ACGAAC is underlined.

E-G) The length of the longest homologous sequence for canonical (C) and non-canonical (NC) are plotted. Here, junctions were considered canonical if they have a 5' end within 20 nucleotides of the TRS-L and a 3' end within 15 nucleotides of a TRS-B. (R) represents random homology lengths. The points for (R) were calculated by first extracting all possible 30 base sequences (30mers) from the SARS-CoV-2 genome, and then assessing the length of the longest homologous sequence between 100,000 random pairs of 30mers that are separated by at least 1000 bases on the genome. Within each column, the relative width of each band represents the relative abundance of junctions with each homology length. The value at the top of each column is the mean homology length.

Figure 5

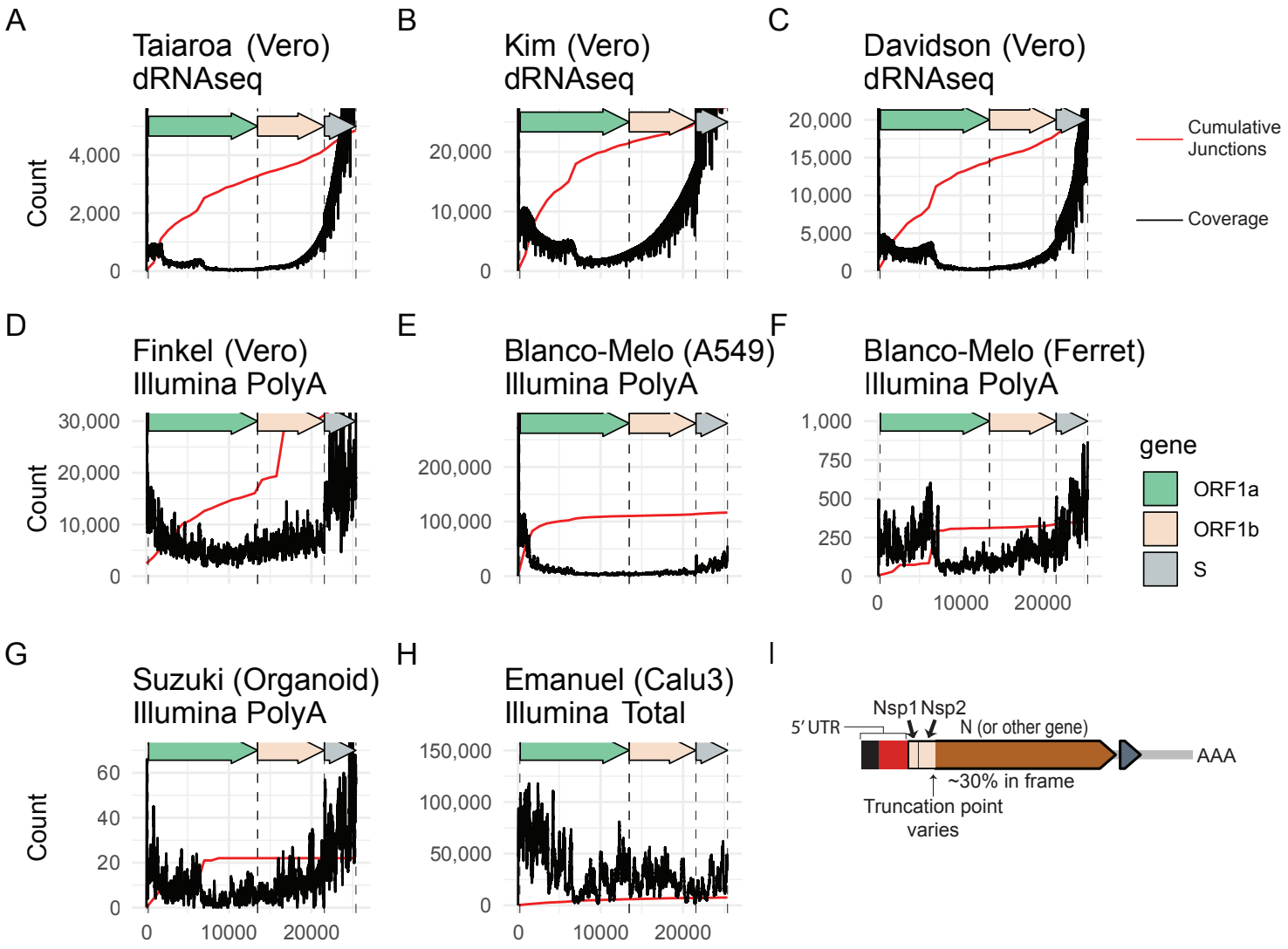

Figure 5. There is evidence of subgenomic RNAs that contain only the 5' end of ORF1a.

A-H) Read coverage (black) and cumulative 5' junctions (red) are plotted for eight independent datasets. The sequencing strategy and sample types are annotated.

I) A schematic of a representative subgenomic RNA that consists of only the 5' region of ORF1a. Pileups showing reads can be found in Supplementary Figure 3.

Figure 6

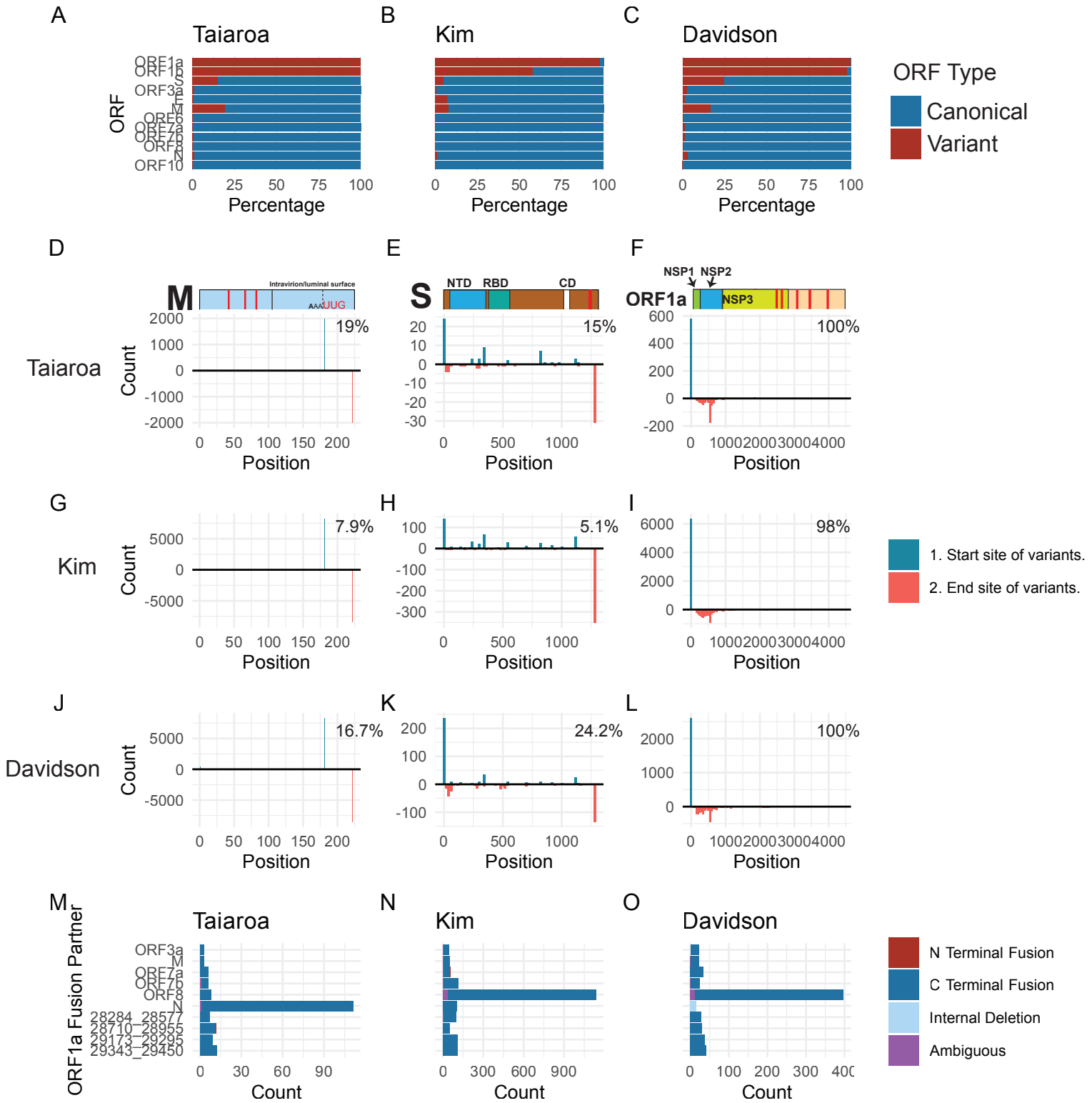

Figure 6. Junctions have the potential to generate variant open reading frames.

A-C) ORFs were predicted directly from transcript-derived reads for the three dRNAseq datasets, and each ORF was aligned against the protein sequences of canonical SARS-CoV-2 genes using the DIAMOND aligner. Variant ORFs were defined as ORFs that were assigned to a canonical SARS-CoV-2 protein but had an unexpected start or stop position, while perfectly-aligning ORFs were considered canonical. The percentage of canonical and variant ORFs for each protein is plotted.

D-L) Schematics of M, N, and ORF1ab are displayed with the approximate location of predicted transmembrane domains labeled in red. A histogram of the start and end sites of variant M, N, and ORF1ab ORFs are displayed. Start sites of each variant ORF are on top, and end sites are on the bottom of each panel. Percentages represent the percentage of each ORF that is variant. Histogram bin-sizes: M, 1; N, 10 ; ORF1ab, 20. NTD: N-terminal domain. RBD: Receptor binding domain. CD: Connector domain. NSP: Nonstructural protein.

M-O) The identity of ORF1a-fusion partners is plotted on the Y axis, with the count of such fusions on the X axis. The top 10 fusion partners for each sample are represented. Color indicates if the fusion partner is on the N and C terminus of ORF1a, if the terminus is ambiguous, or if the fusion is a “self” fusion between an upstream and downstream region of ORF1a. The percentage notes the percent of ORFs assigned to ORF1a that have a fusion.

Supplementary Figure 1

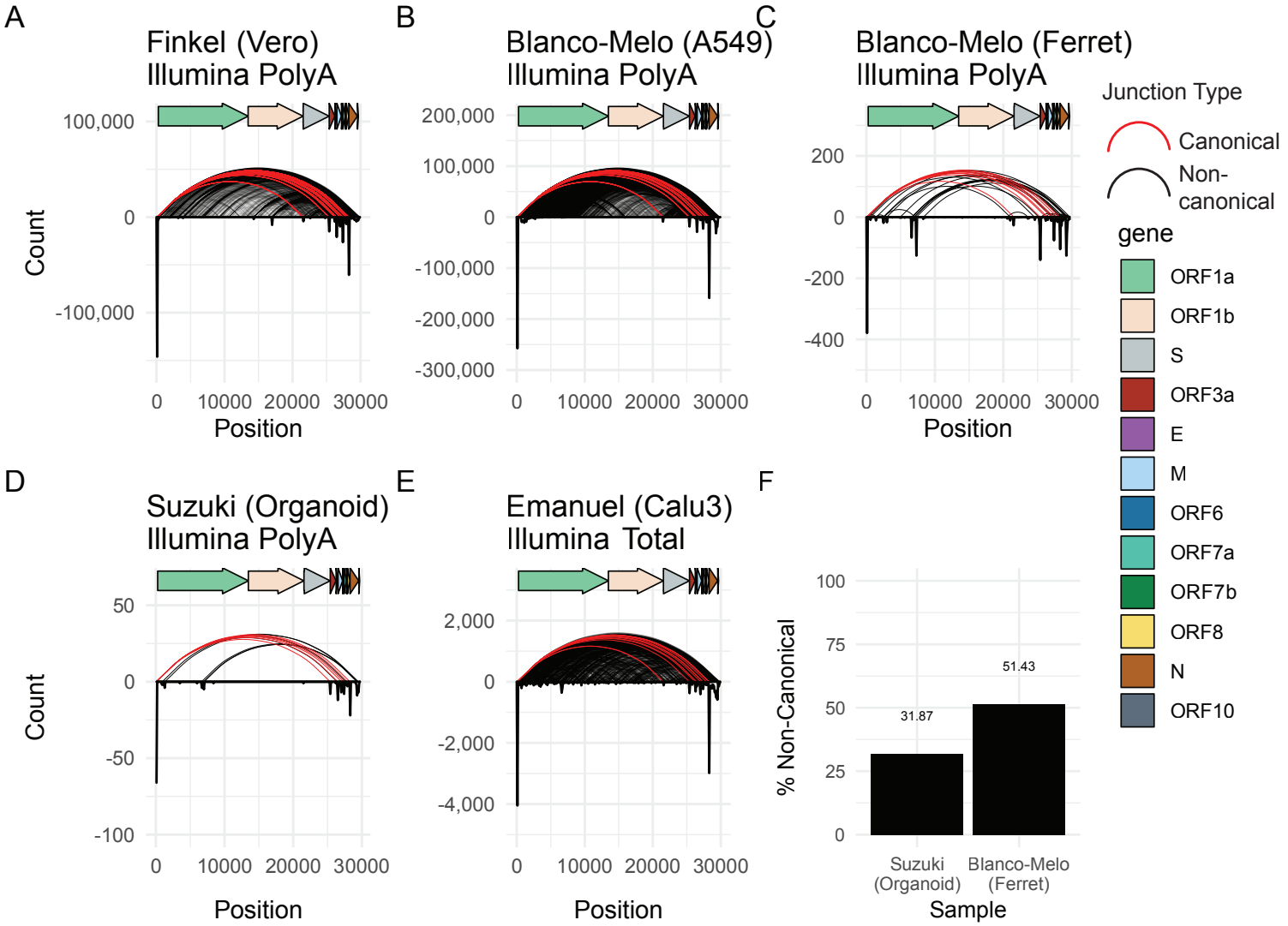

Supplementary Figure 1. There is evidence of non-canonical junctions in diverse datasets.

A-E) For each location on the viral genome, a histogram of 5' and 3' junctions at that position was calculated and plotted as an inverse peak. The histogram bin size is 100 bases, meaning each inverse peak represents the cumulative count of 5' or 3' junctions occurring within that span. Curved lines represent the 5' and 3' locations of junctions that occur at least twice. Red curves represent canonical junctions, black curves represent non-canonical junctions.

F) The percentage of junctions that are canonical in the Suzuki (Bronchial organoids) and Blanco-Melo (Ferret) datasets was determined. Junctions were assigned as canonical if their 5' location was within 20 bases of the TRS-L and their 3' location within 15 bases of a TRS-B, and otherwise assigned as non-canonical.

Supplementary Figure 2

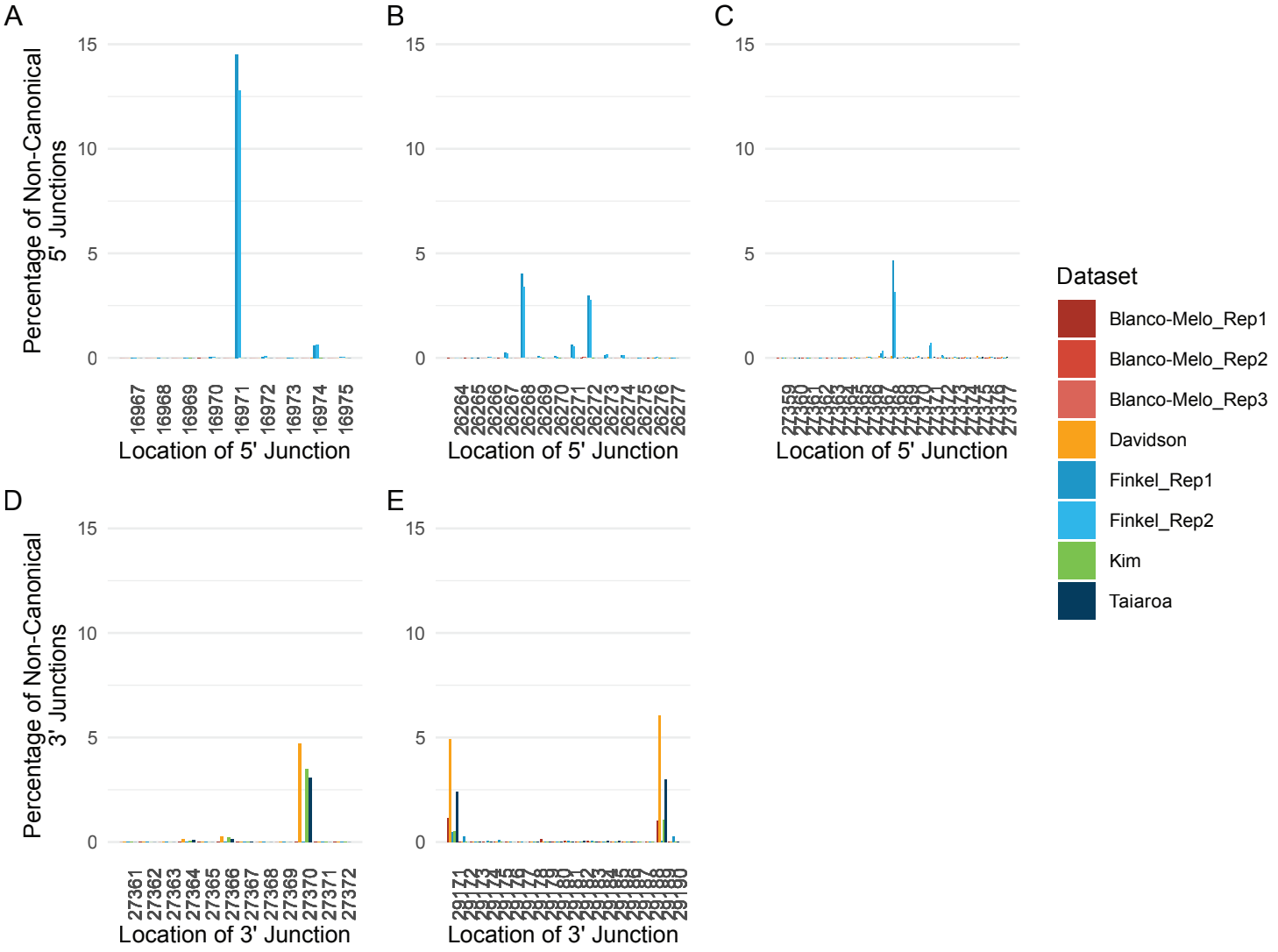

Supplementary Figure 2. There are dataset-specific junctions in Finkel et al.

A-E) The percentage of non-canonical junctions at each SARS-CoV-2 genome position is plotted. Plots A-C show the percentage of 5' junctions at each position, while D-E show the percentage of 3' junctions at each position. The plotted samples include three replicates from Blanco-Melo et al., Davidson et al, two replicate from Finkel et al, and the Kim and Taiaroa et al datasets.

Supplementary Figure 3

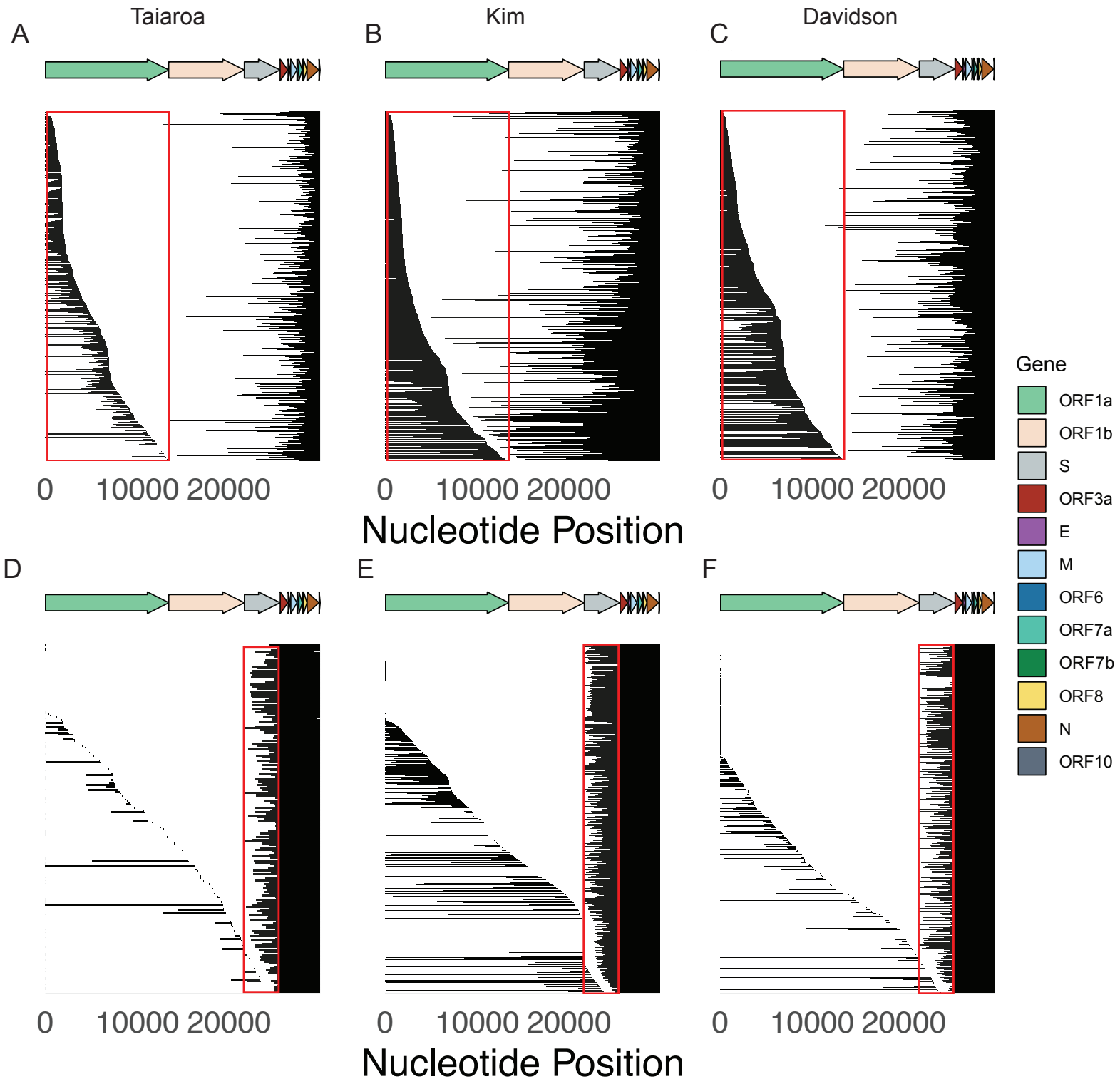

Supplementary Figure 3. Subgenomic RNAs containing non-canonical junctions are present in three independent dRNAseq datasets.

A-F) Subgenomic RNAs with 5' junctions occurring in ORF1a (A-C) or 3' junctions occurring in S (D-F) are plotted for the three dRNAseq datasets. Each row is a read, and regions in black indicate the read contains that sequence.

Supplementary Figure 4

A

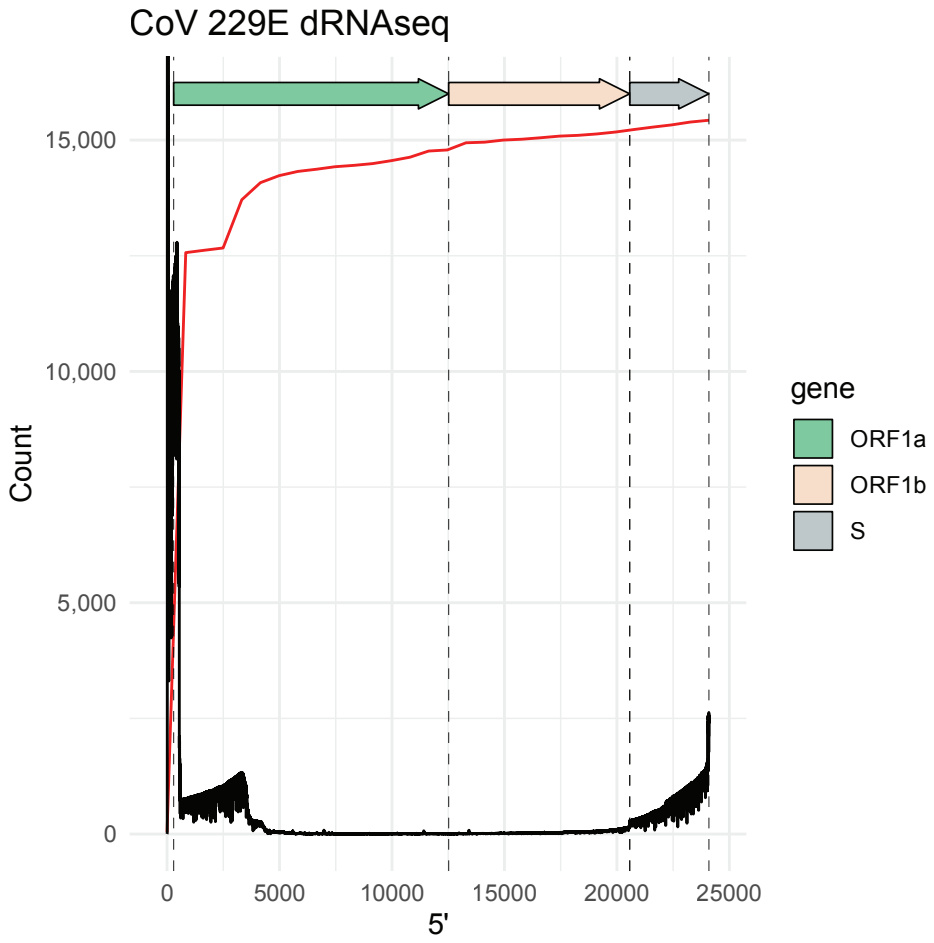

Supplementary Figure 4. There is elevated ORF1A coverage in CoV 229E.

A) Read coverage (black) and cumulative 5' junctions (red) are plotted for dRNAseq data from CoV 229E-infected cells.